Check for updates

Exact quantum dynamics background of dispersion interactions: case study for CH₄·Ar in full (12) dimensions†

Gustavo Avila, [ID] *[a] Dóra Papp, [ID] *[b] Gábor Czakó [ID] *[b] and Edit Mátyus [ID] *[a]

A full-dimensional *ab initio* potential energy surface of spectroscopic quality is developed for the van-der-Waals complex of a methane molecule and an argon atom. Variational vibrational states are computed on this surface including all twelve (12) vibrational degrees of freedom of the methane–argon complex using the GENIUSH computer program and the Smolyak sparse grid method. The full-dimensional computations make it possible to study the fine details of the interaction and distortion effects and to make a direct assessment of the reduced-dimensionality models often used in the quantum dynamics study of weakly-bound complexes. A 12-dimensional (12D) vibrational computation including only a single harmonic oscillator basis function (9D) to describe the methane fragment (for which we use the ground-state effective structure as the reference structure) has a 0.40 cm^{-1} root-mean-square error (rms) with respect to the converged 12D bound-state excitation energies, which is less than half of the rms of the 3D model set up with the $\langle r \rangle_0$ methane structure. Allowing 10 basis functions for the methane fragment in a 12D computation performs much better than the 3D models by reducing the rms of the bound state vibrational energies to 0.07 cm^{-1}. The full-dimensional potential energy surface correctly describes the dissociation of the system, which together with further development of the variational (ro)vibrational methodology opens a route to the study of the role of dispersion forces in the excited methane vibrations and the energy transfer from the intra- to the intermolecular vibrational modes.

I. Introduction

Molecular interactions play an important role in chemistry, biology, and materials science. Through the many-body construction idea[1] of the potential energy surface (PES) of bulk-phase systems the study of molecular interactions is translated to the study of molecular dimers, trimers, and perhaps larger (but still small) clusters.[2–10] Small molecular clusters can be studied in great detail and precision by high-resolution spectroscopic and quantum chemistry and quantum dynamics techniques. A good, 'first' description of the quantum dynamical features of

molecular complexes is provided by the rigid-monomer approximation,[11–14] which allows considerable savings both on the PES development and on the quantum dynamics side. To account for monomer-flexibility effects through the PES representation, the application of effective potential energy cuts (for each monomer vibrational state) provides an improved representation over the rigid-monomer approach while retaining the small number of active vibrational degrees of freedom.[15]

At the same time, monomer flexibility 'effects' are, of course, non-negligible,[16,17] especially for (a) strongly interacting fragments (with strong monomer distortions);[18–20] (b) higher vibrational excitations; (c) monomer vibrational excitations that may correspond to predissociative states of the complex;[21,22] or (d) for symmetry reasons (*i.e.*, degenerate monomer excitations may show a non-trivial coupling with the intermolecular modes). A full account of monomer flexibility in complexes of polyatomic molecules represents a considerable challenge for the current (ro)vibrational methodologies due to the large number of vibrational degrees of freedom and the typically multi-well character of the potential energy landscape.

A generally applicable, 'black-box-type' description of molecular systems with multiple-large amplitude motions is truly challenging, due to (a) the high-dimensionality of the problem,

[a] Institute of Chemistry, ELTE, Eötvös Loránd University, Pázmány Péter sétány 1/A, 1117 Budapest, Hungary. E-mail: Gustavo_Avila@telefonica.net, matyuse@caesar.elte.hu

[b] MTA-SZTE Lendület Computational Reaction Dynamics Research Group, Interdisciplinary Excellence Centre and Department of Physical Chemistry and Materials Science, Institute of Chemistry, University of Szeged, Rerrich Béla tér 1, Szeged H-6720, Hungary. E-mail: dorapapp@chem.u-szeged.hu, gczako@chem.u-szeged.hu

(b) singularities in the kinetic energy operator in the dynamically important region of the coordinate space, (c) a common lack of good zeroth-order models, (d) large basis sets and integration grids being necessary to converge the results, and thus (e) the necessity to attenuate the curse of dimensionality. For semi-rigid molecules there have been efficient methods developed in the past[23] and further major progress has been achieved over the last decade.[24–32] If there is only a single large-amplitude degree of freedom in the system, the reaction-path-Hamiltonian[33] and similar approaches have been successfully used together with semi-rigid techniques.[34,35] There exist efficient, tailor-made approaches developed for particular systems, *e.g.*, for molecular complexes.[4,36] But a general and efficient solution method for systems with multiple large-amplitude motions remains an open problem. For this reason molecular systems with multiple-large amplitude motions represent a current frontier of research in quantum dynamics. The present work contributes to this direction. The family of molecular complexes offers a wide selection of systems with a varying number of large- and small amplitude motions, varying coupling strengths, singularity patterns, *etc.*, and in this way, their study drives methodological development.

In the present work we focus on the floppy, van-der-Waals complex of a methane molecule and an argon atom (with twelve vibrational degrees of freedom), ultimately aiming to reach the predissociative states which belong to the vibrational excitation of the methane fragment, within a full-dimensional vibrational treatment. Due to the weak interactions governing the internal dynamics of the $CH_4 \cdot Ar$ complex, powerful approximations have been introduced in reduced-dimensionality computations, including some methane vibrations, to interpret the high-resolution predissociative spectrum of the complex.[11,37–39] In spite of this earlier experimental and quantum dynamics work (accounting for some methane flexibility) there is not any full-dimensional (12D) potential energy surface available for this system. Hence, the first part of this article is about the development of an *ab initio*, near-spectroscopic quality, full-dimensional PES for $CH_4 \cdot Ar$. The second part reports the first application of this PES in vibrational computations including all 12 vibrational degrees of freedom using the GENIUSH–Smolyak procedure developed by two of us in ref. 40. Note that in ref. 40, a (3D + 9D) PES was used (only including kinetic couplings in the Hamiltonian) in order to be able to test the developed vibrational methodology. In addition to the development and the first applications of a full-dimensional PES for $CH_4 \cdot Ar$, we also take the opportunity to test the rigid-monomer (here 3D) approximation(s), widely used in the study of molecular complexes, with respect to the full-dimensional results.

II. PES development

A. Computational details

1. Benchmark dissociation energies. The geometries of the global (GM) and secondary minima (SM) of the $CH_4 \cdot Ar$ complex are optimized using the explicitly-correlated coupled cluster

singles, doubles, and perturbative triples electronic structure method, CCSD(T)-F12b,[41] with the aug-cc-pVQZ correlation-consistent basis set,[42] followed by harmonic frequency computations at the same level of theory. The resulting equilibrium structures have C_{3v} point-group symmetry forming three (GM) and one (SM) 'H-bond(s)'—or, more precisely, 'H contacts', which modulate the dispersion interaction between Ar and CH_4. To obtain benchmark dissociation energies (D_e) for the GM and SM complexes single-point energy computations are performed at the CCSD(T)-F12b/aug-cc-pVQZ geometries: CCSD(T)-F12b/aug-cc-pV5Z, CCSD(T)[43] and CCSDT(Q)[44] with the aug-cc-pVDZ basis set to obtain post-(T) contributions, and both all-electron (AE) and frozen-core (FC) CCSD(T)-F12b/cc-pCVQZ-F12[45] to determine core-correlation corrections. The FC approach correlates the valence electrons only, whereas in the AE computations the following electrons are also correlated: $1s^2$ for C and $2s^2 2p^6$ for Ar. All the *ab initio* computations are carried out with the Molpro program package,[46] except the CCSD(T) and CCSDT(Q) computations, which are performed using the MRCC program[47] interfaced to Molpro. The final benchmark D_e values are obtained as

$$D_e(\text{CCSD(T)-F12b/aug-cc-pV5Z}) + \delta[\text{CCSDT(Q)}] + \Delta_{\text{core}}, \quad (1)$$

where

$$\delta[\text{CCSDT(Q)}] = D_e(\text{CCSDT(Q)/aug-cc-pVDZ}) \\ - D_e(\text{CCSD(T)/aug-cc-pVDZ}) \quad (2)$$

and

$$\Delta_{\text{core}} = D_e(\text{AE-CCSD(T)-F12b/cc-pCVQZ-F12}) \\ - D_e(\text{FC-CCSD(T)-F12b/cc-pCVQZ-F12}). \quad (3)$$

2. Full-dimensional PES development. A full-dimensional analytic *ab initio* PES, named FullD-2019 PES, is developed based on 15 995 energy points computed at the CCSD(T)-F12b/aug-cc-pVTZ level of theory at geometries covering the configuration space relevant for the interaction between methane and argon. Note that previous test computations by one of us showed that the standard augmented and F12 correlation-consistent basis sets provide similar accuracy for PES development.[48] The geometries used for the PES development are generated by isotropically positioning the Ar atom around the methane unit while atoms of the equilibrium CCSD(T)-F12b/aug-cc-pVTZ methane structure are also randomly displaced. The C–Ar distance is varied between 4 and 20 bohr, and the atoms of methane are displaced in Cartesian coordinates within an interval of [0, 0.95] bohr. The PES is represented by a polynomial expansion in Morse-like variables of the $r_{i,j}$ internuclear distances, $y_{i,j} = \exp(-r_{i,j}/a)$ with $a = 2.0$ bohr, and using a compact polynomial basis that is explicitly invariant under permutation of like atoms.[49,50] The highest total polynomial order applied is 7. The total number of fitting coefficients is 9355. A weighted least-squares fit is performed on the energy points, where a certain energy E relative to the global minimum has a weight of $(E_0/(E_0 + E)) \times (E_1/(E_1 + E))$ with $E_0 = 0.05$ hartree and $E_1 = 0.5$ hartree.

This journal is © the Owner Societies 2020

Phys. Chem. Chem. Phys., 2020, **22**, 2792–2802 | **2793**

Table 1 Benchmark dissociation energies (D_e) in cm^{-1} corresponding to the global (GM) and secondary minimum (SM) structures of the CH$_4$·Ar complex obtained from eqn (1) at CCSD(T)-F12b/aug-cc-pVQZ geometries compared to those obtained on the FullD-2019 PES developed in this study

	AVTZ[a]	AVQZ[b]	Δ_{5Z}[c]	Δ_{core}[d]	Δ[CCSDT(Q)][e]	Final[f]	PES[g]
GM	154.38	149.06	+0.47	+1.40	+1.90	152.83	153.13
SM	103.46	96.79	−0.52	+1.22	+2.03	99.52	102.16

[a] D_e(CCSD(T)-F12b/aug-cc-pVTZ). [b] D_e(CCSD(T)-F12b/aug-cc-pVQZ). [c] D_e(CCSD(T)-F12b/aug-cc-pV5Z) − D_e(CCSD(T)-F12b/aug-cc-pVQZ). [d] D_e(AE-CCSD(T)-F12b/cc-pCVQZ-F12) − D_e(FC-CCSD(T)-F12b/cc-pCVQZ-F12). [e] D_e(CCSD(Q)/aug-cc-pVDZ) − D_e(CCSD(T)/aug-cc-pVDZ). [f] D_e(CCSD(T)-F12b/aug-cc-pV5Z) + Δ_{core} + δ[CCSDT(Q)]. [g] Energy on the PES when the Ar atom was 57 bohr from the equilibrium structure of methane (the interaction energy is less than 0.001 cm^{-1}) relative to the corresponding minimum energy of the PES.

B. Results and discussion

1. Benchmark dissociation energies. In Table 1, we present the benchmark dissociation energies corresponding to the global and secondary minimum geometries of the CH$_4$·Ar complex and compare them to the dissociation energies determined on the newly developed analytic FullD-2019 PES. The correction terms listed in Table 1 allow for estimating the accuracy of the benchmark dissociation energies. The extremely fast basis set convergence of the explicitly-correlated CCSD(T)-F12b method, which is manifested in the Δ_{5Z} corrections of only 0.5 cm^{-1}, ensures that the CCSD(T)-F12b/aug-cc-pV5Z energy is basis-set-converged within about 0.1–0.2 cm^{-1}. The correlation of core electrons increases the dissociation energies by around 1.5 cm^{-1}, and has an estimated uncertainty of 1 cm^{-1}. The δ[CCSDT(Q)]

Table 2 Number of points and root mean square (rms) deviations of the fitting in the chemically interesting energy ranges of the FullD-2019 PES relative to its global minimum

E_{rel} range/cm^{-1}	Number of points	rms/cm^{-1}
0–11 000	11 727	0.66
11 000–22 000	1073	0.90
22 000–55 000	1582	0.95

correlation contributions are also positive values of around 2 cm^{-1} with a similar estimated uncertainty of 1 cm^{-1}. (The uncertainty estimates consider basis set effects and post-(Q) contributions.) Relativistic effects, not taken into account in this work, are supposed to have a smaller contribution than core correlation. Taken together, the uncertainty of the final benchmark dissociation energies is estimated to be ±2 cm^{-1}. The benchmark D_e values, as shown in Table 1, are well reproduced on the new PES with 0.3 cm^{-1} and 2.6 cm^{-1} differences in the case of the global and the secondary minima, respectively. In the case of the global minimum the above agreement is even better than expected due to cancellation of errors as it can be seen from the data of Table 1.

2. Accuracy of the analytic PES. The newly developed full-dimensional analytic PES of the CH$_4$·Ar complex, FullD-2019 PES, features extremely low root mean square (rms) fitting deviations, listed in Table 2, with the rms values being lower than 1 cm^{-1} up to 55 000 cm^{-1} relative to the global minimum of the PES. In accord with these low rms values the one-dimensional energy curves obtained on the PES during the separation of the Ar atom from methane along the C_3 axes of the global and secondary minimum geometries, see Fig. 1, show excellent agreement with the *ab initio* energies. As also seen in Fig. 1, the asymptotic behavior of the weakly-bound CH$_4$·Ar system is also well described by the PES. The asymptotic limits are reached at around 15 bohr from both minima. It is worth emphasizing that the fitted PES reproduces the long-range asymptotic behavior of the high-level *ab initio* data without using any switching function based on the traditional $1/R^6$ dispersion model. Fig. 2 shows that the structural parameters obtained at the minima of the PES agree well with the benchmark CCSD(T)-F12b/aug-cc-pVQZ values. The C–Ar distances are reproduced on the FullD-2019 PES with a difference of 0.003 bohr and 0.029 bohr for the global and the secondary minima, respectively, whereas the C–H bond lengths and the H–C–H angles are practically the same as in the benchmark geometry. Note that the geometry of CH$_4$ is just slightly perturbed in the minima relative to the free CH$_4$ structure; the deformation energy at the global minimum is only 0.05 cm^{-1}. The outstanding accuracy of the FullD-2019 PES is
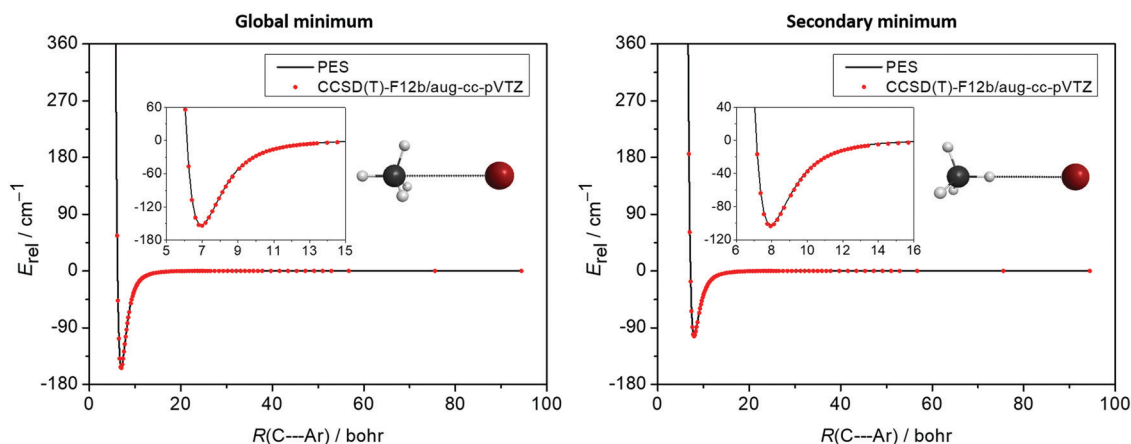
Fig. 1 Potential energy curves along the C_3 axes of the global (left panel) and secondary (right panel) minimum structures scanning the C–Ar distance of the CH$_4$·Ar complex (the CH$_4$ unit is fixed at its CCSD(T)-F12b/aug-cc-pVTZ equilibrium geometry), and showing a comparison between the direct *ab initio* values and cuts of the FullD-2019 PES. The insets show the potential well regions and the corresponding equilibrium geometries.
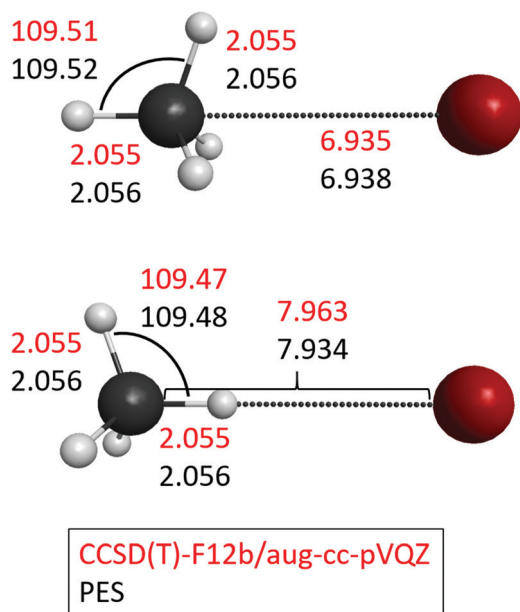
Fig. 2 Geometric parameters of the global (top) and the secondary (bottom) minimum structures of the $CH_4 \cdot Ar$ complex obtained at the CCSD(T)-F12b/aug-cc-pVQZ level of theory (red) and on the FullD-2019 PES (black). Bond lengths are given in bohr and bond angles are given in degrees.

also strengthened by the dissociation energies corresponding to the global and secondary minima, reproducing the benchmark values within 3 cm^{-1} (Table 1). The C–H separation is also scanned on the PES and, as Fig. 3 shows, the FullD-2019 PES describes the C–H stretching motion well up to 30 000 cm^{-1} relative to the global minimum. Furthermore, the potential scans (Fig. 1 and 3) show that the PES function is smooth without any artificial oscillations, proving that the large number of fitting parameters does not cause any overfitting problem.

C. Asymptotic behavior of the PES and comparison with limiting models

The FullD-2019 PES was fitted to *ab initio* points using a permutationally invariant polynomial expansion of Morse variables,
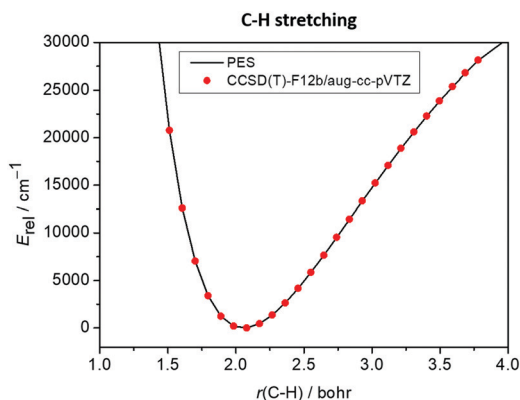

Fig. 3 Potential energy curve along one C–H bond of the CCSD(T)-F12b/aug-cc-pVTZ global minimum geometry while the collinear H atom is separated comparing the direct *ab initio* values and the FullD-2019 PES.

$y_{i,j} = \exp(-r_{i,j}/a)$ (with $a = 2$ bohr), which are exponential functions of distances for all atom–atom pairs.[49] In the present work, we have included in the fit polynomials of $y_{i,j}$ up to degree 7. The advantage of using Morse variables over regular distances is that they ensure non-divergent dissociation asymptotes for large $r_{i,j}$ values. At the same time, one might ask whether the exponentially fast decay of the Morse coordinates allows us to have a correct description of the intermediate range energetics, which, for the present system, is dominated by London dispersion forces, commonly described by a potential energy model, which has not an exponential but a $1/R^6$-type limiting behavior.

The low rms values (Table 2) indicate that the fitting function used for the FullD-2019 PES had sufficient flexibility to reproduce excellently the *ab initio* energies, which, of course, automatically capture all 'interaction effects'. To gain more insight into the short, intermediate, and long-range behavior of the system along the dissociation coordinate, we compare 1D cuts in Fig. 4: the FullD-2019 PES, the Morse potential energy curve, and the best fit of the $-\sigma/R^6$ model (with σ as a constant, fitted parameter) over the $R \in [7.5, 15.5]$ bohr intermediate range.

The Morse potential, $c_0 y_R^0 + c_1 y_R^1 + c_2 y_R^2$, is a second-order polynomial of the y_R Morse variable (defined between the carbon and the argon atoms), and it reproduces excellently the PES valley but it decays too fast to the asymptotic limit (Fig. 4). To reproduce well the asymptotic fall, it is necessary to use a higher than second-order polynomial of the Morse variable, and we found that a polynomial including monomials up to the 7th-order, *i.e.*, up to y_R^7, in the fitting function of the FullD-2019 PES provides an appropriate and automated way to have an excellent overall (short-, intermediate-, and long-range) description of the system.

It is worth pointing out that the difference in the intermediate-range behavior of the Morse (a too fast fall) and
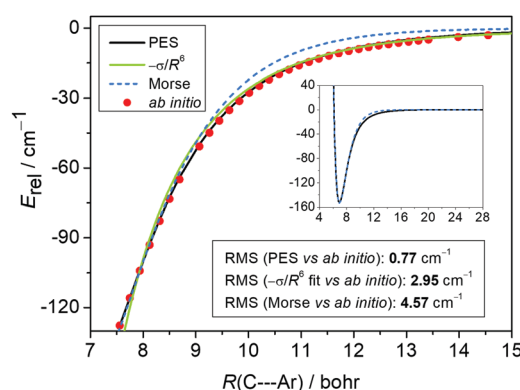
Fig. 4 Long-range interactions: potential energy representations of $CH_4 \cdot Ar$ along the dissociation coordinate showing the 1D cut of the FullD-2019 PES; $-\sigma/R^6$ fit ($\sigma = 2.59741 \times 10^7$ bohr^6 cm^{-1}) to the *ab initio* points in the [7.5, 15.5] bohr range; Morse fit (153.928 cm$^{-1}\{1 - \exp[-0.85(R/\text{bohr} - 6.95)]\}^2 - 153.928$ cm^{-1}); and the CCSD(T)-F12b/aug-cc-pVTZ *ab initio* data. The RMS values correspond to the data in the [7.5, 15.5] bohr interval. The RMS values of the FullD-2019 PES are 0.53 and 0.07 cm^{-1} in the [7.5, 95] and [20, 95] bohr range, respectively, whereas the corresponding RMS deviations for the $-\sigma/R^6$ fits are 1.96 and 0.004 cm^{-1}.

This journal is © the Owner Societies 2020

Phys. Chem. Chem. Phys., 2020, **22**, 2792–2802 | **2795**

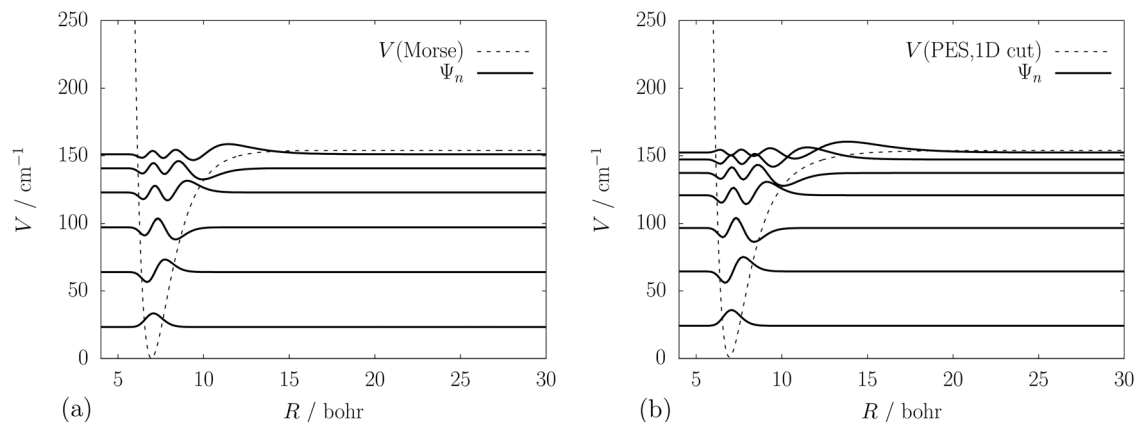**Fig. 5** Vibrational states along the dissociation coordinate (1D model) using (a) the Morse fit, and (b) the 1D cut of the FullD-2019 PES of Fig. 4.

the PES fit (a fall similar to the $1/R^6$ dispersion model) is manifested also in the vibrational structure (Fig. 5). The FullD-2019 PES supports an additional bound vibrational state and the highest energy wave function has a significant amplitude over a much broader range than the highest energy wave function corresponding to the Morse fit. The significant contribution of higher-order polynomials to the PES representation in the long-range asymptotics is observed also in relation to using Morse tridiagonal basis functions (Section IIIB) to solve the vibrational problem: while the low-energy vibrational states can be converged with a small basis set, the highest-energy bound state requires an excessive number of such functions, indicating that there is an important deviation from the too rapidly decaying Morse character.

III. Variational vibrational states

Using the newly developed FullD-2019 PES, the bound vibrational states of the methane–argon complex have been computed using the GENIUSH–Smolyak approach.[40] This extension of the GENIUSH program[51,52] makes it possible to discard basis functions as well as points from the direct product basis and grid, using the Smolyak method,[24,25] thereby attenuating the exponential growth of the computational cost with the vibrational dimensionality. This development makes it possible to solve high-dimensional vibrational problems, for which or for, at least, parts of which a good zeroth-order representation can be constructed.

In the case of the $CH_4 \cdot Ar$ complex, a good zeroth-order approximation is obtained for the methane fragment by using normal coordinates $(q_1, q_2, \ldots, q_9)$ and harmonic oscillator basis functions. The relative motion of the fragments is described by spherical polar coordinates, $(R, \cos\theta, \phi)$ similarly to ref. 40.

The GENIUSH program requires the definition of the internal coordinates (and the body-fixed, BF, frame) by specifying the Cartesian coordinates in the BF frame with respect to the internal coordinates. The program uses this information to construct the kinetic energy operator (KEO) terms in an

automated fashion.[51] The usual Cartesian coordinate expression of the (generalized) normal coordinates, $q_j \in (-\infty, \infty)$, is

$$r_{i\alpha} = c_{i\alpha}^{\text{ref}} + \sum_{j=1}^{9} l_{i\alpha,j} q_j , \qquad (4)$$

with $i = 1(H), 2(H), 3(H), 4(H), 5(C)$ and $\alpha = 1(x), 2(y), 3(z)$. The $l_{i\alpha,j}$ linear combination coefficients and the $c_{i\alpha}^{\text{ref}}$ reference structure can be chosen by convenience (as a special case, they can be obtained from the harmonic analysis of the PES at the equilibrium structure). In the present work, we chose $c_{i\alpha}^{\text{ref}}$ to reproduce not the equilibrium structure (which could be one of the minima of $CH_4 \cdot Ar$ or the isolated CH_4 minimum), but to reproduce the tetrahedral methane structure for which the C–H distance corresponds to the effective structure of the methane zero-point vibration with $\rho := r_{\text{eff}} = 2.067337961$ bohr,[40]

$$(\mathbf{c}_1^{\text{ref}})^{\text{T}} = \frac{\rho}{\sqrt{3}}(1, 1, 1)$$

$$(\mathbf{c}_2^{\text{ref}})^{\text{T}} = \frac{\rho}{\sqrt{3}}(1, -1, -1)$$

$$(\mathbf{c}_3^{\text{ref}})^{\text{T}} = \frac{\rho}{\sqrt{3}}(-1, -1, 1) \qquad (5)$$

$$(\mathbf{c}_4^{\text{ref}})^{\text{T}} = \frac{\rho}{\sqrt{3}}(-1, 1, -1)$$

$$(\mathbf{c}_5^{\text{ref}})^{\text{T}} = (0, 0, 0).$$

This choice accounts for anharmonicity effects on the structure of the methane fragment already in the coordinate definition. (Note that here we used an effective structure determined in previous work[40] which reproduces the B_0 value corresponding to the methane PES of ref. 53.) Using an effective methane structure corresponding to the ground-state vibration instead of the equilibrium structure for the reference structure of the generalized normal coordinates slightly speeds up the convergence of the vibrational energies with respect to the methane basis. In the 'complete basis' limit, the precise reference structure becomes irrelevant, of course.

The Cartesian coordinates of the argon atom are defined with respect to the carbon atom placed at the origin, using the

2796 | *Phys. Chem. Chem. Phys.*, 2020, **22**, 2792–2802

This journal is © the Owner Societies 2020

spherical polar coordinates, $R \in [0, \infty)$ bohr, $\cos \theta \in [-1,1]$, and $\phi \in [0, 2\pi)$,

$$r_{6x} = R \sin \theta \cos \phi$$

$$r_{6y} = R \sin \theta \sin \phi \qquad (6)$$

$$r_{6z} = R \cos \theta.$$

In the last step of the coordinate definition, the $r_{i\alpha}$ Cartesian structure, eqn (4)–(6), is shifted to the center of mass of the methane–argon complex. Throughout this work, atomic masses are used, $m(H) = 1.00782503223$ u, $m(C) = 12$ u, and $m(Ar) = 39.9623831237$ u.[54]

In the forthcoming subsections, we first test cuts of the FullD-2019 PES in lower-dimensional vibrational computations. We report the results of 9D computations carried out for the methane fragment (with the argon atom fixed at a large distance), and observations from 1D (R) and 2D ($\cos \theta, \phi$) radial and angular model computations are summarized. The experience gathered from these tests is combined to determine the optimal parameters for the 12D computation, which is presented in the last subsection. It is important to emphasize that in the final computations we include all 12 vibrational degrees of freedom in the variational vibrational treatment, but we chose the coordinates, in particular, the reference structure of the generalized normal coordinate definition, so that they provide an excellent description for the bound atom–molecule vibrations, which are dominated by the methane zero-point state.

A. Isolated methane vibrations

The energy levels of the methane molecule were computed on the FullD-2019 PES with the argon atom fixed at a 30 bohr distance from the center of mass of the CH_4 fragment. The atom–molecule interaction is (almost) negligible (less than 0.05 cm^{-1}) at this separation. For the variational computations, we started out from a direct-product basis set of harmonic oscillator functions, $\phi_{n_1}(q_1) \ldots \phi_{n_9}(q_9)$ ($n_i = 0, 1, \ldots, i = 1, \ldots 9$), which was pruned according to the simple condition $n_1 + \ldots + n_9 \leq b$. An integration grid (much) smaller than the naïve direct-product grid was defined using the Smolyak scheme.[24,25] In short, the grid points were chosen to integrate exactly the identity matrix and also polynomials of up to a maximum total degree of 5 with the basis functions included in the pruned basis set.[40] The pruning parameter, the size of the basis, and the size of the Smolyak grid are listed in Table 3. The convergence rate with respect to the basis and grid size and benchmark results for the vibrational energies of CH_4 are shown in Table 4.

Using the $b = 10$ basis-pruning parameter, the energies are converged within 0.01 cm^{-1} up to (and including) the pentad of CH_4. The 9690.62 cm^{-1} zero-point vibrational energy (ZPVE) on the FullD-2019 PES is in good agreement with the 9691.56 cm^{-1} value corresponding to the T8 force field of Schwenke and Partridge.[55] The root-mean-square (rms) deviation of the converged vibrational excitation energies with respect to their counterparts deduced from experiments[56] is 2.88 cm^{-1}, which is excellent given that this is a purely *ab initio* PES, which was developed not specifically for an

Table 3 Basis set and integration grid parameters used to describe the methane fragment

b^a	H^b	$N_{bas}{}^c$	$N_{Smol}{}^d$
0	11^e	1	163^e
1	12^e	10	871^e
2	13	55	3481
3	14	220	11 833
4	15	715	35 929
5	16	2002	97 561
6	17	5005	241 201
7	18	11 440	556 707
8	19	24 310	1 202 691
9	20	48 620	2 440 227
10	21	92 378	4 718 595

^{a} Basis pruning condition, $n_1 + \ldots + n_9 \leq b$. ^{b} Grid pruning condition, $i_1 + \ldots + i_9 \leq H$ (for details, see for example ref. 40 and references therein). We chose $H = D - 1 + b + 3$ (here $D = 9$) to integrate exactly not only the overlap but also polynomials of a maximum degree of 5 with all basis functions included in the pruned basis set. ^{c} The number of basis functions in the pruned basis set is $N_{bas} = (b + 9)!/(b!9!)$. ^{d} The number of points in the Smolyak grid corresponding to the selected H value. ^{e} When using the FullD-2019 PES with $b = 0$ ($b = 1$), we observed that $H = 11$ ($H = 12$) is not sufficient to recover the correct degeneracy of the methane vibrations (especially the E states were affected). So, in the end, we used $H = 12$ ($H = 13$) and $N_{Smol} = 871$ ($N_{Smol} = 3481$) for $b = 0$ ($b = 1$).

isolated methane molecule but for the methane–argon complex. Note that these 'isolated methane' energies were obtained using the FullD-2019 PES with the argon atom fixed at a large distance from the methane molecule.

Assessment of smaller basis sets (smaller b values) is important for planning the 12D computations. The bound states of the $CH_4 \cdot Ar$ complex are dominated by the zero-point state of methane, hence $b = 3$ should be an excellent compromise for computing the intermolecular (atom–molecule) states accurately. The computation of predissociative states corresponding to excited vibrational states of methane will require at least $b = 6$–7, which assumes further development of the vibrational methodology.

B. Intermolecular radial representation

There are several possibilities to describe the vibrational motion along the methane–argon distance. One can use $\mathcal{L}_n^{(\alpha)}$ generalized Laguerre basis functions (with $\alpha = 2$)[21,57] or a Morse tridiagonal basis set. The Laguerre basis set may be a better choice for computing predissociative states, whereas the Morse tridiagonal basis set offers a more compact alternative for bound states. In the present work, we used the Morse tridiagonal basis set parameterized with the $D = 150$ cm^{-1}, $\alpha = 0.65$, and $\gamma = 0.00033$ values,[18,40,58–60] which gave a good Morse fit to the cut of the FullD-2019 PES at the equilibrium (global minimum) structure of all other coordinates. Since $CH_4 \cdot Ar$ is an isotropic complex, this radial basis is expected to perform well over the entire range of the angular coordinates. The convergence tests suggest that 13 Morse functions with 15 quadrature points for R allow us to converge the 3D($R, \cos \theta, \phi$) and 12D bound-state energies within 0.01 cm^{-1}.

C. Intermolecular angular representation

For the $\cos \theta$ coordinate, we use sin-cot-DVR (DVR, discrete variable representation) basis functions and points,[61] while

This journal is © the Owner Societies 2020

Phys. Chem. Chem. Phys., 2020, **22**, 2792–2802 | **2797**

Table 4 Convergence of the zero-point and vibrational excitation energies, in cm^{-1}, up to and including the pentad of CH$_4$ with respect to the (pruned) basis set size using the GENIUSH–Smolyak approach[40] and the FullD-2019 PES with an argon–methane distance fixed at $R = 30$ bohr. The benchmark energies corresponding to this PES are given in the $\tilde{\nu}(b = 10)$ column

Γ^a	Label^b	$\Delta_0{}^c$	$\Delta_1{}^c$	$\Delta_2{}^c$	$\Delta_3{}^c$	$\Delta_4{}^c$	$\Delta_5{}^c$	$\Delta_6{}^c$	$\Delta_7{}^c$	$\Delta_8{}^c$	$\Delta_9{}^c$	$\tilde{\nu}(b = 10)^c$	δ^d	$\tilde{\nu}_{\exp}{}^e$
A_1	0000	43.79	42.42	40.06	1.79	0.60	0.52	0.04	0.01	0.01	0.00	9690.62	—	—
F_2	0001	—	9.61	7.68	41.19	2.14	0.27	0.54	0.06	0.01	0.01	1310.60	0.16	1310.76
E	0100	—	5.76	5.55	39.20	1.76	0.18	0.50	0.04	0.01	0.01	1531.47	1.86	1533.33
A_1	0002	—	—	37.74	56.88	43.69	4.60	1.24	0.64	0.11	0.02	2586.02	1.02	2587.04
F_2	0002	—	—	29.71	54.22	45.63	3.86	1.12	0.66	0.10	0.02	2613.61	0.65	2614.26
E	0002	—	—	19.70	51.49	45.00	3.13	0.94	0.62	0.08	0.01	2623.93	0.69	2624.62
F_2	0101	—	—	23.55	51.84	40.55	3.20	0.97	0.56	0.07	0.01	2828.08	2.24	2830.32
F_1	0101	—	—	17.14	49.64	43.22	2.87	0.87	0.59	0.07	0.01	2844.38	1.70	2846.08
A_1	1000	—	89.70	34.44	66.84	10.68	1.63	1.38	0.27	0.05	0.02	2912.36	4.12	2916.48
F_2	0010	—	107.24	38.27	69.89	11.81	1.76	1.50	0.29	0.05	0.03	3014.47	5.02	3019.49
A_1	0200	—	—	15.09	49.17	41.73	2.73	0.82	0.56	0.06	0.01	3059.25	4.40	3063.65
E	0200	—	—	13.75	47.58	41.39	2.48	0.78	0.55	0.06	0.01	3061.06	4.08	3065.14
rms													2.88	

^{a} Label of the irreducible representation of the T_d point group of methane. ^{b} '$n_1n_2n_3n_4$' normal mode label. ^{c} Deviation from the $\tilde{\nu}(b = 10)$ benchmark value, $\Delta_k = \tilde{\nu}(b = k) - \tilde{\nu}(b = 10)$. ^{d} $\delta = \tilde{\nu}_{\exp} - \tilde{\nu}(b = 10)$. ^{e} Vibrational energies deduced from experiments are taken from ref. 56.

Fourier basis functions are used for the ϕ angle. Test computations suggest that 23 sin-cot-DVR functions for $\cos\theta$ and 21 Fourier functions with 24 quadrature points for ϕ will be sufficient to converge the 3D(R, $\cos\theta$, ϕ) and 12D vibrational excitation energies better than 0.01 cm^{-1}.

D. Full-dimensional (12D) vibrational states and comparison with 3D models

All vibrational bound states of the CH$_4$·Ar complex on the newly developed FullD-2019 PES are listed in Table 5. The intermolecular basis set corresponding to the (R, $\cos\theta$, ϕ) coordinates is sufficiently large to converge all vibrational excitation energies better than 0.01 cm^{-1}. In order to find the smallest necessary intramolecular methane basis set (characterized with the b basis-pruning parameter), we have carried out 12D computations with an increasing basis set size on the methane fragment corresponding to the $b = 0$, 1, 2, and 3 value. Concerning the ZPVE, we think that the $b = 3$ 12D result is *ca.* 1–2 cm^{-1} larger (our approach is nearly variational) than the exact result, similarly to the $b = 3$ ZPVE value of isolated methane (Table 4). Concerning the intermolecular vibrational excitation energies, we could efficiently rely on the cancellation of error in the relative vibrational energies, and thus a rather small methane basis set was sufficient to achieve the 0.01 cm^{-1} convergence goal for the excitation energies.

It is interesting to consider the convergence of the excitation energies with respect to b. The 12D computation with $b = 0$, which corresponds to a single(!) basis function on the methane fragment, has an rms error of 0.40 cm^{-1}. This rms value is *ca.* half of the rms error of a well-converged 3D computation imposing rigorous geometrical constraints with an $\langle r \rangle_0$ methane structure (*vide infra*). A 12D computation with $b = 1$, which includes 10 basis functions for the methane fragment, has an rms of 0.07 cm^{-1}. Finally, our 0.01 cm^{-1} convergence goal is achieved for the $b = 2$ and $b = 3$ pruning parameter values.

Concerning the computational cost, the $b = 0$ and $b = 1$ computations took 10 and 20 hours (using 20 processor cores) and required 6 and 8 GB of memory, respectively. The 12D

$b = 3$ ($b = 2$) computations took 42 (13) days on 50 (20) cores and required 80 (30) GB of memory. As it was indicated already in the footnote to Table 3, we had to use a larger grid size for $b = 0$ and 1 than we had originally anticipated, which slightly increased the cost of the computation. Furthermore, the condition number of the Hamiltonian matrix in the current representation is very large (due to the application of sin-cot-DVR basis functions, there are grid points which are very close to the singularities of the KEO), which implies an increased number of Lanczos iteration steps. We anticipate reduction of the computational cost with further development.

Table 5 also shows the result of 3D, rigid-monomer computations, in which only the R, $\cos\theta$, and ϕ degrees of freedom were treated as active coordinates. The '3D($\langle r \rangle_0$)' column corresponds to reduced-dimensionality results in which rigorous geometrical constraints were imposed on the methane's structure (referred to as 'the reduction in the Lagrangian' or 'reduction in the $\boldsymbol{g}$ matrix' in ref. 51 and constructed automatically in GENIUSH). The methane was fixed at a regular tetrahedral structure with $\langle r_{C-H} \rangle_0$, which we calculated as the expectation value of the C–H distance using the isolated methane's ground-state wave function on the present PES. The vibrational excitation energies of this 3D model have a relatively large, 0.93 cm^{-1}, rms with respect to the converged 12D result. Furthermore, this 3D model (erroneously) predicts an additional, triply degenerate, bound state below the dissociation asymptote, which can be explained by the slightly different B_0 value corresponding to this model.

In the '3D($\langle B \rangle_0$)' column, we report the bound vibrational energies obtained with an 'adjusted' 3D model. While using the $\langle r_{C-H} \rangle_0$ value for defining the 3D cut of the PES, we adjusted the C–H distance in the KEO to reproduce the $\langle B \rangle_0$ effective rotational constant of this PES in 2D coupled-rotor computations.[13,57] This model reproduces the correct number of bound states and has a smaller, 0.32 cm^{-1}, rms than the 3D model with the rigorous geometrical constraints.

In relation to these 3D models, we conclude that a 12D computation performed with a single 9D basis function for methane ($b = 0$) is on a par with the 3D($\langle B \rangle_0$) model. If we allow

Table 5 All bound-state vibrational energies, $\tilde{\nu}$ in cm^{-1}, of $CH_4 \cdot Ar$, computed with the GENIUSH–Smolyak approach[40] and the FullD-2019 PES developed in the present work

#	Assignment[a]			12D[b]				3D($\langle r \rangle_0$)[c]		3D($\langle B \rangle_0$)[d]	
	j	n_R	Γ	Δ_0	Δ_1	Δ_2	$\tilde{\nu}(b=3)$	$\tilde{\nu}_{3D}$	δ^e	$\tilde{\nu}_{3D}$	δ^e
0[f]	0	0	A_1	66.10	40.67	38.32	9754.40	54.30	—	54.38	—
1–3	1	0	F_2	0.21	0.03	0.00	8.68	8.65	0.04	8.87	−0.19
4	0	1	A_1	0.10	0.01	0.00	29.88	29.80	0.07	29.89	−0.01
5–7	2	0	F_2	0.29	0.01	−0.01	31.63	30.84	0.79	31.29	0.35
8–9	2	0	E	0.40	0.05	0.01	32.34	31.65	0.69	32.21	0.13
10–12	1	1	F_2	0.21	0.02	0.01	45.76	45.27	0.49	45.63	0.13
13	0	2	A_1	0.06	0.00	0.01	54.79	54.54	0.26	54.66	0.14
14–16	2	1	F_2	0.50	0.05	0.00	56.80	55.92	0.88	56.58	0.22
17–18	2	1	E	0.39	0.05	0.02	65.64	64.92	0.72	65.49	0.14
19–21	3	0	F_2	0.80	0.08	−0.01	66.08	64.52	1.56	65.72	0.36
22–24	1	2	F_1	0.33	0.03	0.01	67.86	66.86	1.00	67.45	0.41
25	0	3	A_1	0.30	0.02	0.00	72.62	71.19	1.42	72.02	0.60
26	3	0	A_1	0.31	0.02	0.01	75.23	74.63	0.60	74.97	0.26
27–29	2	2	F_2	0.29	0.02	0.00	77.73	76.46	1.28	77.11	0.63
30–32	1	3	F_2	0.32	0.03	0.01	82.25	81.71	0.54	82.17	0.08
33	0	4	A_1	−0.12	−0.01	0.02	87.53	87.06	0.47	87.18	0.35
34–36	1	4	F_2	0.23	0.03	0.02	91.42	90.57	0.84	91.07	0.35
37–38	2	4	E	0.34	0.04	0.02	91.61	90.80	0.81	91.38	0.23
39	0	5	A_1	−0.42	−0.26	0.03	95.44	94.75	0.69	95.02	0.42
40–42	3	3	F_2	0.97	0.10	0.00	95.69	94.07	1.61	95.42	0.26
43	0	6	A_1	−0.09	0.03	0.03	99.11	98.21	0.90	98.72	0.39
44–46				—	—	—	—	99.32	—	—	—
rms[g]				0.40	0.07	0.01			0.93		0.32

[a] Characterization of the computed states using the 3D wave functions of the 3D($\langle B \rangle_0$) column. j: angular momentum quantum number of the methane fragment and the relative diatom in the $[j,j]_{00}$ dominant coupled-rotor (CR) function;[57] n_R: vibrational excitation along R; Γ: irrep label of the $T_d(M)$ molecular symmetry group of the complex based on the CR assignment and irrep decomposition.[57] [b] $\Delta_k = \tilde{\nu}(b=k) - \tilde{\nu}(b=3)$, where b is the pruning parameter of the methane basis, the intermolecular radial and angular representations are defined in the text, and is sufficient for converging the figures shown in the table. [c] 3D computation using rigorous geometrical constraints with a regular tetrahedral methane structure with $\langle r_{C-H} \rangle_0 = 2.093624127$ bohr (used both in the KEO and in the PES). [d] 3D computation using an 'adjusted' r_{fit}(C–H) = 2.072988169 bohr C–H distance in the KEO, which in a 2D coupled-rotor computation[13,57] reproduces the $\langle B \rangle_0 = 5.212508664$ cm^{-1} effective rotational constant corresponding to this PES. To define the 3D cut of the PES, we used $\langle r_{C-H} \rangle_0$. [e] $\delta = \tilde{\nu}(b=3) - \tilde{\nu}_{3D}$. [f] Zero-point vibration of the complex. The vibrational excitation energies, #: 1, 2, 3,..., are given with respect to this value. [g] Root-mean-square deviation from the $\tilde{\nu}(b=3)$ (12D) result.

only 10 functions for the methane fragment ($b = 1$) in the 12D computation, the 12D result clearly outperforms the 3D excitation energies, without increasing the computational cost dramatically.

In order to rationalize these numerical observations, we may distinguish between 'static' and 'dynamical' contributions from the methane's vibrations to the atom–molecule energy levels. The static contribution is due to the fact that the isolated molecule's effective (average) structure, due to anharmonicity of methane's vibrations, is different from the equilibrium structure. In 3D computations, this effect is accounted for by fixing the methane's structure at an effective structure instead of the equilibrium structure. In 12D computations, we have 'built in' this static effect in the coordinate definition (using generalized normal coordinates) in order to speed up convergence with respect to the methane's basis size.

The dynamical contribution is due to the coupling of the methane's vibrations with the intermolecular dynamics. This dynamical coupling, which is often small but non-negligible, requires a full-dimensional treatment. In the case of the methane–argon complex, we observe that using only the ground and all singly excited (9D) harmonic oscillator functions captures almost all dynamical effects, but well-converged excitation energies assume at least 220 (9D) harmonic oscillator functions, corresponding to the $n_1 + n_2 + \ldots + n_9 \leq 3$ pruning condition, for the methane fragment.

From a numerical point of view, it is necessary to mention that the 12D and 3D results are close, within 1–2 cm^{-1}, to the vibrational states reported in ref. 11 (Table 4) on a 3D PES developed using symmetry-adapted perturbation theory and an effective (ro)vibrational Hamiltonian some 20 years ago. The present work reports a fully *ab initio* quantum dynamics study of the system in full dimensionality and its further extension to predissociative states may reveal larger deviations from the effectively designed approach of ref. 11 and 37. There are also experimental results in the predissociative range,[38,39] which will make the comparison more interesting. Furthermore, the methodology recently developed and used in the present work is not designed specifically for very weakly interacting atom–molecule complexes, but it can be used for a greater variety of molecular systems and it fits in a series of recent efforts made for systematic development of general 'black-box-type' (ro)vibrational quasi-variational methods, applicable to molecular complexes or any other molecular systems, of high vibrational dimensionality and with multiple large-amplitude motions.

IV. Summary and conclusions

The present work reports the development of a full-dimensional, near-spectroscopic quality *ab initio* potential energy surface for

the van-der-Waals complex of the methane molecule and an argon atom. The PES development is accompanied by the computation of all vibrational bound states of this complex including all (12) vibrational degrees of freedom in a near-variational treatment using the GENIUSH program and the Smolyak algorithm. The vibrational excitation energies obtained within a 12D treatment were used to assess traditional 3D (rigid-monomer) approaches. With further development of the quantum dynamics methodology, full-dimensional computations will become more widespread and applicable to floppy molecules or molecular complexes over a broad energy range.

Conflicts of interest

There are no conflicts of interest to declare.

Acknowledgements

References

1 J. N. Murrell, S. Carter, S. C. Farantos, P. Huxley and A. J. C. Varandas, *Molecular Potential Energy Functions*, New York, Wiley, 1984.

2 M. Quack and M. A. Suhm, Potential energy surfaces, quasiadiabatic channels, rovibrational spectra, and intra-molecular dynamics of $(HF)_2$ and its isotopomers from quantum Monte Carlo calculations, *J. Chem. Phys.*, 1991, **95**, 28.

3 M. Quack, J. Stohner and M. A. Suhm, Vibrational dynamics of $(HF)_n$ aggregates from an *ab initio* based analytical (1 + 2 + 3)-body potential, *J. Mol. Struct.*, 1993, **294**, 33.

4 G. C. Groenenboom, E. M. Mas, R. Bukowski, K. Szalewicz, P. E. S. Wormer and A. van der Avoird, The pair and three-body potential of water, *Phys. Rev. Lett.*, 2000, **84**, 4072–4075.

5 W. Cencek, K. Szalewicz, C. Leforestier, R. van Harrevelt and A. van der Avoird, An accurate analytic representation of the water pair potential, *Phys. Chem. Chem. Phys.*, 2008, **10**, 4716–4731.

6 Y. Wang and J. M. Bowman, *Ab initio* potential and dipole moment surfaces for water. II. Local-monomer calculations of the infrared spectra of water clusters, *J. Chem. Phys.*, 2011, **134**, 154510.

7 G. R. Medders, V. Babin and F. Paesani, A critical assessment of two-body and three-body interactions in water, *J. Chem. Theory Comput.*, 2013, **9**, 1103.

8 V. Babin, G. R. Medders and F. Paesani, Development of a "first principles" water potential with flexible monomers. II: Trimer potential energy surface, third virial coefficient, and small clusters, *J. Chem. Theory Comput.*, 2014, **10**, 1599.

9 P. Jankowski, G. Murdachaew, R. Bukowski, O. Akin-Ojo, C. Leforestier and K. Szalewicz, *Ab initio* water pair potential with flexible monomers, *J. Phys. Chem. A*, 2015, **119**, 2940–2964.

10 U. Góra, W. Cencek, R. Podeszwa, A. van der Avoird and K. Szalewicz, Predictions for water clusters from a first-principles two-and three-body force field, *J. Chem. Phys.*, 2014, **140**, 194101.

11 T. G. A. Heijmen, P. E. S. Wormer, A. van der Avoird, R. E. Miller and R. Moszynski, The rotational and vibrational dynamics of argon-methane. I. A theoretical study, *J. Chem. Phys.*, 1999, **110**, 5639.

12 J. Sarka, A. G. Császár, S. C. Althorpe, D. J. Wales and E. Mátyus, Rovibrational transitions of the methane-water dimer from intermolecular quantum dynamical computations, *Phys. Chem. Chem. Phys.*, 2016, **18**, 22816.

13 J. Sarka, A. G. Császár and E. Mátyus, Rovibrational quantum dynamical computations for deuterated isotopologues of the methane-water dimer, *Phys. Chem. Chem. Phys.*, 2017, **2**, 15335.

14 M. P. Metz, K. Szalewicz, J. Sarka, R. Tóbiás, A. G. Császár and E. Mátyus, Molecular dimers of methane clathrates: *ab initio* potential energy surfaces and variational vibrational states, *Phys. Chem. Chem. Phys.*, 2019, **21**, 13504.

15 M. Jeziorska, P. Jankowski, K. Szalewicz and B. Jeziorski, On the optimal choice of monomer geometry in calculations of intermolecular interaction energies: Rovibrational spectrum of Ar-HF from two- and three-dimensional potentials, *J. Chem. Phys.*, 2000, **113**, 2957.

16 X. G. Wang and T. Carrington, Jr, Using monomer vibrational wavefunctions as contracted basis functions to compute rovibrational levels of an H_2O-atom complex in full dimensionality, *J. Chem. Phys.*, 2017, **146**, 104105.

17 X. G. Wang and T. Carrington, Jr, Using monomer vibrational wavefunctions to compute numerically exact (12D) rovibrational levels of water dimer, *J. Chem. Phys.*, 2018, **148**, 074108.

18 G. Avila and E. Mátyus, Full-dimensional (12D) variational vibrational states of $CH_4 \cdot F^-$: interplay of anharmonicity and tunneling, *J. Chem. Phys.*, 2019, **151**, 154301.

19 C. Fábri, A. G. Császár and G. Czakó, Reduced-dimensional quantum computations for the rotational-vibrational dynamics of $F^- - CH_4$ and $F^- - CH_2D_2$, *J. Phys. Chem. A*, 2013, **117**, 6975.

20 R. Wodraszka, J. Palma and U. Manthe, Vibrational Dynamics of the $CH_4 \cdot F^-$ Complex, *J. Phys. Chem. A*, 2012, **116**, 11249.

21 D. Papp, J. Sarka, T. Szidarovszky, A. G. Császár, E. Mátyus and M. Hochlaf, *et al.*, Complex rovibrational dynamics of the $Ar \cdot NO^+$ complex, *Phys. Chem. Chem. Phys.*, 2017, **19**, 8152–8160.

22 P. M. Felker and Z. Bacic, Weakly bound molecular dimers: Intramolecular vibrational fundamentals, overtones, and tunneling splittings from full-dimensional quantum calculations using compact contracted bases of intramolecular

2800 | *Phys. Chem. Chem. Phys.*, 2020, **22**, 2792–2802

This journal is © the Owner Societies 2020

and low-energy rigid-monomer intermolecular eigenstates, *J. Chem. Phys.*, 2019, **151**, 024305.

23 J. M. Bowman, S. Carter and X. Huang, MULTIMODE: A code to calculate rovibrational energies of polyatomic molecules, *Int. Rev. Phys. Chem.*, 2003, **22**(3), 533–549.

24 G. Avila and T. Carrington Jr., Nonproduct quadrature grids for solving the vibrational Schrödinger equation, *J. Chem. Phys.*, 2009, **131**(17), 174103.

25 G. Avila and T. Carrington Jr., Using nonproduct quadrature grids to solve the vibrational Schrödinger equation in 12D, *J. Chem. Phys.*, 2011, **134**(5), 054126.

26 G. Avila and T. Carrington Jr., Using a pruned basis, a non-product quadrature grid, and the exact Watson normal-coordinate kinetic energy operator to solve the vibrational Schrödinger equation for C_2H_4, *J. Chem. Phys.*, 2011, **134**(6), 064101.

27 A. Leclerc and T. Carrington, Calculating vibrational spectra with sum of product basis functions without storing full-dimensional vectors or matrices, *J. Chem. Phys.*, 2014, **140**(17), 174111.

28 P. S. Thomas and T. Carrington, An intertwined method for making low-rank, sum-of-product basis functions that makes it possible to compute vibrational spectra of molecules with more than 10 atoms, *J. Chem. Phys.*, 2017, **146**(20), 204110.

29 T. Halverson and B. Poirier, One million quantum states of benzene, *J. Phys. Chem. A*, 2015, **119**(50), 12417–12433.

30 J. Brown and T. Carrington, Using an expanding nondirect product harmonic basis with an iterative eigensolver to compute vibrational energy levels with as many as seven atoms, *J. Chem. Phys.*, 2016, **145**(14), 144104.

31 N. K. Madsen, I. H. Godtliebsen, S. A. Losilla and O. Christiansen, Tensor-decomposed vibrational coupled-cluster theory: Enabling large-scale, highly accurate vibrational-structure calculations, *J. Chem. Phys.*, 2018, **148**, 024103.

32 A. Baiardi and M. Reiher, Large-scale quantum-dynamics with matrix product states, *J. Chem. Theory Comput.*, 2019, **15**, 3481.

33 W. H. Miller, N. C. Handy and J. E. Adams, Reaction path Hamiltonian for polyatomic molecules, *J. Chem. Phys.*, 1980, **72**, 99.

34 J. M. Bowman, X. Huang, N. C. Handy and S. Carter, Vibrational levels of methanol calculated by the reaction path version of MULTIMODE, using an *ab initio*, full-dimensional potential, *J. Phys. Chem. A*, 2007, **111**, 7317.

35 D. Lauvergnat and A. Nauts, Quantum dynamics with sparse grids: A combination of Smolyak scheme and cubature. Application to methanol in full dimensionality, *Spectrochim. Acta, Part A*, 2014, **119**, 18–25.

36 C. Leforestier, *Philos. Trans. R. Soc., A*, 2012, **370**, 2675.

37 T. G. A. Heijmen, T. Korona, R. Moszynski, P. E. S. Wormer and A. van der Avoird, *Ab initio* potential-energy surface and rotationally inelastic integral cross sections of the Ar-CH_4 complex, *J. Chem. Phys.*, 1997, **107**, 902.

38 R. E. Miller, T. G. A. Heijmen, P. E. S. Wormer, A. van der Avoird and R. Moszynski, The rotational and vibrational dynamics of argon-methane. II. Experiment and comparison with theory, *J. Chem. Phys.*, 1999, **110**, 5651.

39 M. Wangler, D. A. Roth, I. Pak, G. Winnewisser, P. E. S. Wormer and A. van der Avoird, The high-resolution spectrum of the Ar-CH_4 complex in the 7 μm region: measurement and *ab initio* calculation, *J. Mol. Spectrosc.*, 2003, **222**(1), 109.

40 G. Avila and E. Mátyus, Toward breaking the curse of dimensionality in (ro)vibrational computations of molecular systems with multiple large-amplitude motions, *J. Chem. Phys.*, 2019, **150**, 174107.

41 T. B. Adler, G. Knizia and H. J. Werner, A simple and efficient CCSD(T)-F12 approximation, *J. Chem. Phys.*, 2007, **127**, 221106.

42 T. H. Dunning, Jr, Gaussian basis sets for use in correlated molecular calculations. I. The atoms boron through neon and hydrogen, *J. Chem. Phys.*, 1989, **90**, 1007.

43 K. Raghavachari, G. W. Trucks, J. A. Pople and M. Head-Gordon, A fifth-order perturbation comparison of electron correlation theories, *Chem. Phys. Lett.*, 1989, **157**, 479.

44 M. Kállay and J. Gauss, Approximate treatment of higher excitations in coupled-cluster theory, *J. Chem. Phys.*, 2005, **123**, 214105.

45 D. E. Woon and T. H. Dunning Jr, Gaussian basis sets for use in correlated molecular calculations. V. Core-valence basis sets for boron through neon, *J. Chem. Phys.*, 1995, **103**, 4572.

46 H.-J. Werner, P. J. Knowles, G. Knizia, F. R. Manby and M. Schütz *et al.*, Molpro, version 2015.1, a package of *ab initio* programs, see http://www.molpro.net.

47 MRCC, a quantum chemical program suite written by M. Kállay, Z. Rolik, I. Ladjánszki, L. Szegedy, B. Ladóczki, J. Csontos and B. Kornis, *J. Chem. Phys.*, 2011, **135**, 104111, See also Z. Rolik, M. Kállay, as well as: www.mrcc.hu.

48 G. Czakó, I. Szabó and H. Telekes, On the choice of the *ab initio* level of theory for potential energy surface developments, *J. Phys. Chem. A*, 2014, **118**, 646.

49 B. J. Braams and J. M. Bowman, Permutationally invariant potential energy surfaces in high dimensionality, *Int. Rev. Phys. Chem.*, 2009, **28**, 577.

50 J. M. Bowman, G. Czakó and B. Fu, High-dimensional *ab initio* potential energy surfaces for reaction dynamics calculations, *Phys. Chem. Chem. Phys.*, 2011, **13**, 8094.

51 E. Mátyus, G. Czakó and A. G. Császár, Toward black-box-type full- and reduced-dimensional variational (ro)vibrational computations, *J. Chem. Phys.*, 2009, **130**, 134112.

52 C. Fábri, E. Mátyus and A. G. Császár, Rotating full- and reduced-dimensional quantum chemical models of molecules, *J. Chem. Phys.*, 2011, **134**, 074105.

53 X. G. Wang and T. Carrington Jr, Using experimental data and a contracted basis Lanczos method to determine an accurate methane potential energy surface from a least squares optimization, *J. Chem. Phys.*, 2014, **141**(15), 154106.

54 J. S. Coursey, D. J. Schwab, J. J. Tsai and R. A. Dragoset, Atomic Weights and Isotopic Compositions (version 4.1), National Institute of Standards and Technology, Gaithersburg, MD, 2015, http://physics.nist.gov/Comp last accessed on 12 May 2018.

This journal is © the Owner Societies 2020

Phys. Chem. Chem. Phys., 2020, **22**, 2792–2802 | **2801**

55 D. W. Schwenke and H. Partridge, Vibrational energy levels for CH$_4$ from an *ab initio* potential, *Spectrochim. Acta*, 2001, **57**, 887.

56 A. V. Nikitin, M. Rey and V. G. Tyuterev, Rotational and vibrational energy levels of methane calculated from a new potential energy surface, *Chem. Phys. Lett.*, 2011, **501**, 179.

57 D. Ferenc and E. Mátyus, Bound and unbound rovibrational states of the methane-argon dimer, *Mol. Phys.*, 2019, **117**, 1694.

58 H. Wei and T. Carrington, Jr, The discrete variable representation of a triatomic Hamiltonian in bond length-bond angle coordinates, *J. Chem. Phys.*, 1992, **97**, 3029.

59 B. R. Johnson and W. P. Reinhardt, Adiabatic separations of stretching and bending vibrations: Application to H$_2$O, *J. Chem. Phys.*, 1986, **85**(8), 4538–4556.

60 J. Tennyson and B. T. Sutcliffe, The *ab initio* calculation of the vibrational-rotational spectrum of triatomic systems in the close-coupling approach, with KCN and H$_2$Ne as examples, *J. Chem. Phys.*, 1982, **77**(8), 4061–4072.

61 G. Schiffel and U. Manthe, On direct product based discrete variable representations for angular coordinates and the treatment of singular terms in the kinetic energy operator, *Chem. Phys.*, 2010, **374**(1), 118–125.